minerals

MDPI

Article

Aqua Traiana, a Roman Infrastructure Embedded in the Present: The Mineralogical Perspective

Michela Botticelli, Laura Calzolari, Caterina De Vito, Silvano Mignardi and Laura Medeghini *

Department of Earth Sciences, Sapienza University of Rome, Piazzale A. Moro, 5, 00185 Rome, Italy; michela.botticelli@uniroma1.it (M.B.); laura.calzolari@uniroma1.it (L.C.); caterina.devito@uniroma1.it (C.D.V.); silvano.mignardi@uniroma1.it (S.M.)

* Correspondence: laura.medeghini@uniroma1.it; Tel.: +39-064991-4926

Abstract: Construction materials from the internal ducts of *Aqua Traiana*, a still operative Roman aqueduct built in 109 AD to supply water to Rome, were characterized by optical microscopy (OM), scanning electron microscopy (SEM-EDS), X-ray powder diffraction (XRPD) and electron microprobe analysis (EMPA). Petrographic analysis and XRPD revealed that mortar aggregates are compatible with Vitruvius' *harena fossicia* and allowed the distinction of the original mortars from those of the 17th-century papal restoration. The first showed an amorphous binder while the latter have a typical lime binder. By SEM-EDS and EMPA, the microstructure of mortar aggregates was analyzed and the composition of specific minerals quantified. Microanalysis testifies the Romans' great expertise in the selection of pozzolanic building materials, giving evidence of the possible use of local tuffs from the Sabatini Volcanic District. It also confirms the exploitation of red pozzolan from the Roman Magmatic Province, specifically from the Alban Hills district. OM also proves a high compatibility with local supplies for bricks and *cocciopesto*. Of these, the first were fired at moderately low temperature, while the latter show an amorphous binder as in the original Trajan mortars. All building materials thus stand for similar technological choices and a coeval production.

Keywords: Roman mortars; aqueduct; microanalysis; red pozzolan; Sabatini Volcanic District

Citation: Botticelli, M.; Calzolari, L.; De Vito, C.; Mignardi, S.; Medeghini, L. *Aqua Traiana*, a Roman Infrastructure Embedded in the Present: The Mineralogical Perspective. *Minerals* **2021**, *11*, 703. https://doi.org/10.3390/min11070703

Academic Editors: Daniel Albero Santacreu, José Cristóbal Carvajal López and Adrián Durán Benito

Received: 2 June 2021
Accepted: 26 June 2021
Published: 29 June 2021

1. Introduction

Knowledge on ancient societies develops through the study of customs, traditions, beliefs and relationships with other populations. Important information can be obtained by the analysis of the materials these societies produced. In this perspective, archaeometry has recently paid increasing attention to the mineralogical and chemical study of geomaterials [1–10] to reconstruct technological knowledge and skills acquired by ancient populations.

Roman aqueducts are the greatest expression of these competencies, material awareness being merged with the creation of architectural solutions to ensure survival over time. Although these monuments reflect the set of engineering knowledge of the past, historical sources dealing with their raw materials and supplies are few: Vitruvius' *De Architectura*, Pliny the Elder's *Naturalis Historia* or Strabo's *Geographica* [11]. Similarly, archaeometric studies taking into consideration material analysis on aqueducts are rare. Mortars and bricks from the Antioch aqueduct of Syria (Turkey) have been most recently analyzed to identify their production technology and deterioration [12]; mortars and plasters from the aqueduct of Naxos island (Greece) have been studied to define their hydraulic features [13]; finally, mortars, pilasters and arches of the ancient aqueduct of Carthage have been characterized [14]. Even the Italian literature is scarce: in the Roman aqueduct of Padua only stone materials were characterized [15]; Rizzo et al. [16] characterized the hydraulic mortars used in Pantelleria aqueducts and finally ceramic pipes of the Roman aqueduct of Raiano (L'Aquila) were analyzed to identify its raw materials [17].

Aqua Traiana is one of the few still functioning Roman aqueducts and the characterization study hereby presented is a unique opportunity to document its building materials.

The aqueduct, with its 57-km route from Lake Bracciano to Rome and the strong difference in height between the starting and arrival point (from 320 to 72 m asl), is a perfect example of Roman engineering skills (Figure 1a). Inaugurated in 109 AD, *Aqua Traiana* was built to supply energy to the mills located on the Janiculum (eastern part of the city of Rome). The main duct is variable, both in size and height, and it is characterized by a mixture of construction methods and materials. During barbarian invasions, the aqueduct was damaged several times. It was finally restored by Pope Paul V, between 1609 and 1612 [18–20]. Since that moment, it has never stopped functioning and supplying water to Rome.

The present study evaluates the mineralogical and physicochemical composition of mortars, *cocciopesto* and bricks from the *Aqua Traiana* to define the building technology. Of these, *cocciopesto* is the term applied to a mortar containing either crushed terracotta or pozzolan [21]. A multianalytical approach was applied including optical microscopy (OM) in thin section and X-ray powder diffraction (XRPD). Scanning electron microscopy with energy dispersive X-ray spectroscopy (SEM-EDS) and electron microprobe analysis (EMPA) were then applied to determine chemical composition and microstructure of the mortars.

The results obtained from the different samples allow a complete characterization of the materials used in the monument and the comparison among those used in the Trajan Era and the ones related to the restauration of Pope Paul V.

Brief Geological Setting

Lake Bracciano is part of the Sabatini Volcanic District, which belongs to the Roman Comagmatic Province [22]. The high-K feature of these products has been related to a metasomatized mantle source, i.e., to a phlogopite-bearing peridotite recording subduction-related fluids and/or melting processes [23–25]. The occurrence of silica-undersaturated ultrapotassic rocks (e.g., leucite-bearing) is related to the subduction of carbonate-rich pelites [26]. Volcanic activity was mainly characterized by widespread pyroclastic flows and sub-Plinian to Plinian fallout, the activity area (ca. 1800 Km^2) having originated the Bracciano system (W) and the Sacrofano system (E) [22,27].

The Sabatini Volcanic District is characterized by volcanic rocks ranging from leucite-tephrites to leucite- and haüyne-phonolites. The activity of the area can be divided in five main phases, which generated the volcanic products shown in Figure 1a.

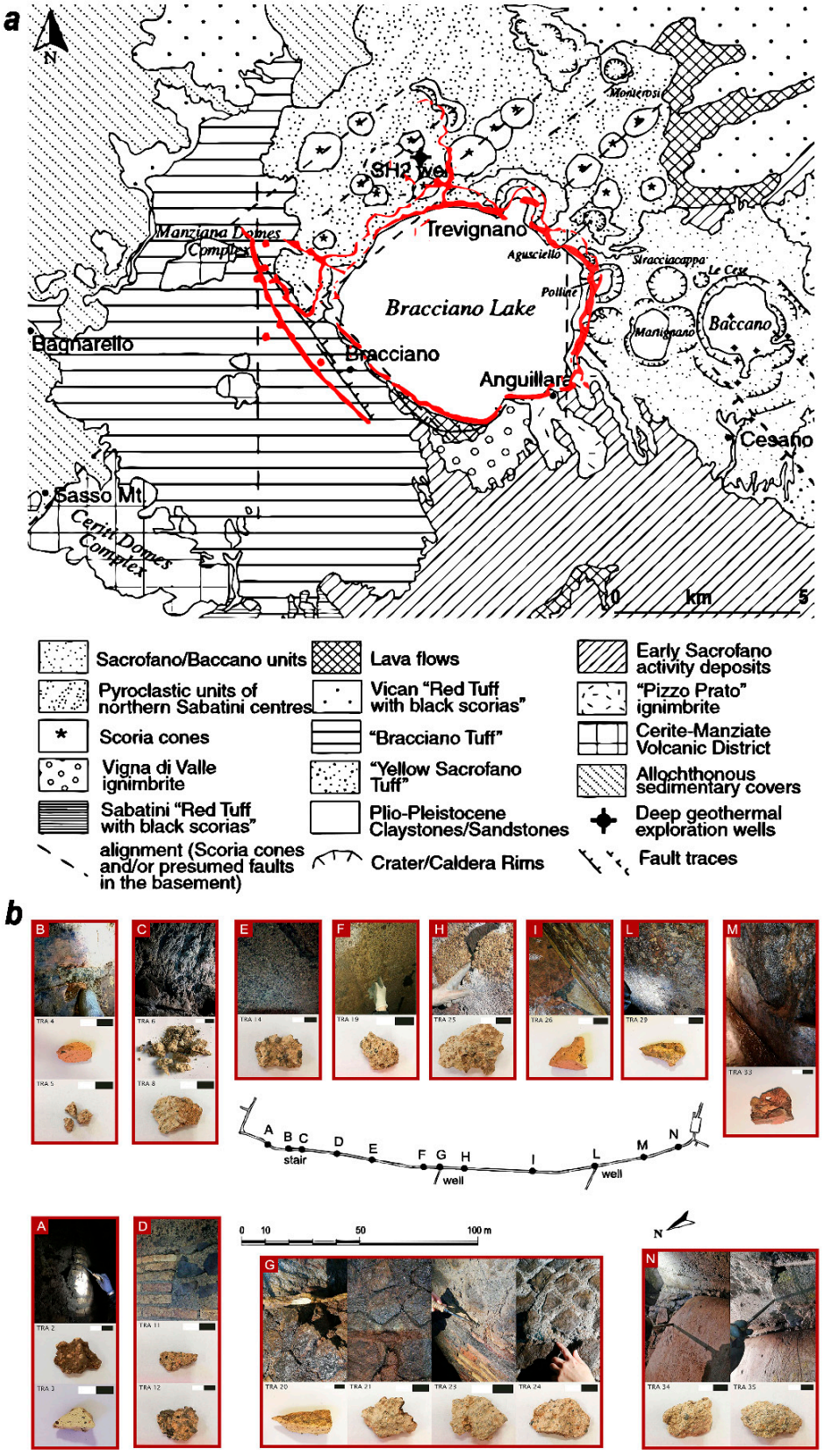

Figure 1. (**a**) Geological map of the Sabatini Volcanic District, modified after [28]: the light red line represents the path of the Trajan aqueduct around Lake Bracciano; (**b**) segment of the aqueduct with the location of each sampling point (**A**–**N**) and corresponding sample (Table 1).

Among them, the Tufo Giallo della Via Tiberina (yellow tuff of Via Tiberina, TGdVT) leucite phono-trachytic pyroclastic succession includes lower (LTGdVT) and upper (UTGdVT) sequences, Tufo Giallo di Prima Porta (yellow tuff of Prima Porta, TGdPP) and the Grottarossa Pyroclastic Sequence [22,29]; above it the emplacement of extensive airfall tuffs and ashes interbedded with surges and minor pyroclastic flow units corresponds to the Sacrofano stratified tuffs, alternating with sporadic lava flows; a large pyroclastic-flow forms the Tufo Rosso a Scorie Nere (red tuff with black scoria, TRaSN); finally, a succession of pumice and scoria fall deposits underlies the Tufo Giallo di Sacrofano (yellow tuff of Sacrofano, TGdS) [30].

Table 1. List of samples analyzed, with the reference period and sampling point.

Sample	Dating	Description
mortars		
TRA 2	Trajan Age	Mortar between bricks
TRA 5	Trajan Age	Mortar between the bricks of the stairs near TRA 4
TRA 6	Papal restoration	Mortar of the vault that covers the access stair
TRA 8	Trajan Age	Mortar between leucitite blocks (between the stair and the vault)
TRA 11	Trajan Age	Mortar in the junction between leucitite blocks and *opus latericium*
TRA 12	Trajan Age	Mortar of the vault, over sample TRA 11
TRA 14	Trajan Age	Mortar of the vault
TRA 19	Trajan Age	Mortar of the vault
TRA 21	Trajan Age	Mortar between leucitite blocks in the well
TRA 23	Trajan Age	Mortar between the bricks
TRA 24	Trajan Age	Mortar between leucitite blocks in the well
TRA 25	Trajan Age	Mortar of the vault
TRA 34	Papal restoration	Plaster on the wall
TRA 35	Papal restoration	Mortar of the vault over TRA 34
cocciopesto		
TRA 29	Trajan Age	*Cocciopesto* from the wall
TRA 33	Trajan Age	*Cocciopesto* from the floor
brick		
TRA 3	Trajan Age	Brick near TRA 2
TRA 4	Trajan Age	Brick of the stairs
TRA 20	Trajan Age	Brick from the floor of the well
TRA 26	Trajan Age	Bipedal brick from the floor

2. Materials and Methods

2.1. Samples

Samples of ancient mortars, bricks and *cocciopesto* (Table 1, Figure 1b) were collected inside a secondary duct of Trajan's aqueduct, at Settebotti-Trevignano Romano, in the northern area of Lake Bracciano (Rome, Italy). Fourteen mortar samples belong to different types of masonry (mortars between bricks in *opus latericium*, mortars between stone blocks in *opus reticulatum* or the hydraulic plaster). They are also representative of different building phases (Trajan Age and papal restoration), as recognized by the archaeologists based on macroscopic features, stratigraphic context and construction phase; two *cocciopesto* (or *opus signinum*) fragments were collected from the covering of the duct, whereas four brick fragments were sampled from both the masonry and the bipedal bricks used on the floor.

2.2. Experimental Methods

A preliminary macroscopic analysis was performed by the naked eye on dried samples to define the colour and size of the aggregates and the possible presence of additives.

Thin sections were then analyzed by a Zeiss D-7082 Oberkochen polarized optical microscope. Microscopic analysis in both parallel (PPL) and crossed polarized light (XPL) was performed according to Pecchioni et al. [31] and the normal 12/83 [32] for mortars, through which it was also possible to qualitatively estimate the binder/aggregate ratio and porosity by visual comparison. Whitbread's criteria [33] were indeed used for brick and *cocciopesto* fragments.

The identification of material providing hydraulicity is easy by OM. However, if this component is finely ground or interference colours are similar to that of the matrix, microstructural analysis combined with chemical investigations can help [31]. Hence, SEM-EDS investigation was carried out on representative mortar samples. Based on microscopic analysis, macroscopic features and discrimination given by the archaeologists, two Papal samples (TRA 6 and TRA 35) and five Trajan samples (TRA 2, TRA 11, TRA 12, TRA 21 and TRA 23) were analyzed. A FEI Quanta 400 scanning electron microscope coupled with energy dispersive spectroscopy was used to define the microstructure of the samples and chemical composition of the aggregates and possibly highlight different microchemical features between original and restoration materials.

EMPA was also carried out on samples representative of the different function of the mortar: in the junction between leucitite blocks and *opus latericium* (TRA 11); between leucitite blocks in the well (TRA 21) and between bricks (TRA 23). A Cameca SX50 microprobe was used, equipped with five wavelength-dispersive spectrometers and operating at 15 kV accelerating voltage, 15 nA beam current and 10 μm beam size. Element peaks and background were measured with counting times of 20 s and 10 s respectively. Wollastonite was used as a reference standard for Si (TAP, thallium (acid) phthalate crystal) and Ca (XET, pentaerythritol crystal), augite for Mg (TAP), corundum for Al (TAP), jadeite for Na (TAP), rutile for Ti (XET), fayalite for Fe (LIF, lithium fluoride), rhodonite for Mn (LIF), orthoclase for K (XET), chalcopyrite for Cu (LIF), galena for Pb (XET), cassiterite for Sn (XET), apatite for P (XET), barite for Ba (XET) and sphalerite for Zn (LIF). Matrix corrections were calculated by the PAP method with software supplied by the Microbeams Services [34,35]. The relative analytical error was 1% for major elements and it increased as their concentration decreased [36,37]. The detection limits under the specified working condition ranged between 0.01 and 0.1 wt %.

Finally, a small amount of each mortar sample was finely ground in an agate mortar for XRPD analysis by a Bruker D8 focus diffractometer with CuKα radiation, operating at 40 kV and 30 mA. The following instrumental set-up was chosen: 3–60° 2θ range and a scan step of 0.02° 2θ/2 s. Data processing, including semiquantitative analysis based on the "Reference Intensity Ration Method", was performed using XPowderX software.

3. Results and Discussion

3.1. Mortars

The preliminary macroscopic analysis highlighted that the mortars samples are hard and compact, i.e., resistant and not friable. They are characterized by a binder fraction varying in colour from beige to yellow and a pozzolan-based aggregate with tuff-ash fragments. Grains vary in size and shape (from rounded to subrounded) and are mainly represented by dark, reddish and yellow tuff fragments. Specifically, Trajan samples present a light-grey, whitish colour binder fraction.

Optical microscopy first permitted to distinguish the microstructure of the binder: a carbonate one with micritic texture and high birefringence for the papal samples and an amorphous gel-like cementing matrix in the Trajan mortars. In addition, OM analysis allowed the estimation of the binder/aggregate ratio. Papal samples show a ratio of 1:2, whereas Trajan Age samples have a binder/aggregate ratio of 1:3 or near this value.

XRPD spectra of papal restoration samples show very abundant calcite related to the binder. Minerals mainly related to the aggregate, which are possibly linked to a volcanic origin, are present in variable amount: clinopyroxene; K-feldspar, anorthoclase or sanidine; and zeolites, like analcime. Clay minerals are absent. On the contrary, most of the samples,

which correspond to the original Trajan Age samples, are characterized by the absence of calcite and a more abundant presence of clinopyroxene, clay minerals being present or in trace (Table 2). Specifically, the absence of calcite in these samples could be due to a complete portlandite consuming during the pozzolanic reaction (preventing calcite formation) or connected to alteration processes [38].

Table 2. Mineral assemblage of mortar samples and relative abundances (++++ very abundant; +++ abundant; ++ common; + present; t trace; - not detected), calculated by the reference intensity ratios (RIR) method in XPowderX. Anl: analcime, Cpx: clinopyroxene, Bt: biotite, Cal: calcite, Fsp: feldspar, Lct: leucite, Qtz: quartz, Cbz: chabazite, Pl: plagioclase, Amp: amphibole.

Sample	Anl	Cpx	Bt	Cal	Fsp	Clays	Lct	Qtz	Cbz	Pl	Amp
TRA 2	+++	++	+	-	++	+	-	t	t	-	-
TRA 5	+++	++++	t	-	+	t	-	-	-	t	-
TRA 6	-	+	+	++++	+	-	+	t	-	-	-
TRA 8	++++	++++	t	-	t	-	-	-	-	-	-
TRA 11	+++	++++	++	-	t	t	-	-	-	-	-
TRA 12	+++	++	t	-	++++	t	t	-	-	-	-
TRA 14	++++	+	++	-	+++	t	-	-	-	+	-
TRA 19	+++	++	t	-	++++	t	-	-	-	-	-
TRA 21	++	t	t	-	++++	t	-	-	-	-	-
TRA 23	+++	++++	t	-	++	t	-	-	tr	-	-
TRA 24	++	t	t	-	++++	t	-	-	-	-	t
TRA 25	+++	++	+	-	+	+	-	-	-	+++	-
TRA 34	t	+	t	++++	+	-	-	-	-	-	-
TRA 35	++	++	t	+++	+++	-	-	-	-	-	-

Additionally, based on the amount of alkali feldspars, two subgroups of Trajan samples can be described. One subgroup has K-feldspars generally very abundant in samples coming from the vault or between leucitite blocks in proximity of the first wall (see Figure 1b, samples TRA 12, TRA 14 and TRA 19 from the vault and TRA 21, TRA 23 and TRA 24 between leucitite blocks in the well or bricks nearby). Another subgroup indeed shows K-feldspars as present or in trace, mainly coming from the stairs (TRA 2, TRA 5 and TRA 8 in Figure 1b). Micaceous minerals, specifically biotite, are ubiquitous in lower amount. A feldspathoid typical of the Roman volcanic activity, leucite, was identified only in sample TRA 6, as already found by OM. Traces of clinopyroxene were found in TRA 14 and quartz in sample TRA 11.

Petrographic and SEM-EDS analysis highlighted that the aggregate is mainly composed of volcanic rock fragments, such as pyroclastic rock fragments with pozzolanic behavior. The pozzolanic material mainly consists of pumice clasts, tuff and lava fragments with primary phenocrysts surrounded by a vitreous fine-ash matrix. Porosity, size, shape and distribution of the aggregate are highly variable among the samples (Figure 2).

Specifically, it was possible to identify different inclusions belonging to the aggregate fraction. The pyroclastic rock fragments with porphyritic texture, variable porosity, sphericity, shape and colour ranging from brown to red or rarely yellow can be defined as pozzolanic tuff-like materials (Figure 2). This type of aggregate is the most abundant in all samples and less diffusive in samples TRA 6 and TRA 34. They are either highly porphyric, with augite-crystals, or sometimes surrounded by illuvial clays (PYR Figure 2c).

Some big porous reddish-brown fragments with a very low porphyritic character and leucite microcrystals showing star-like habit were also recognized by OM as red pozzolan (RP in Figure 2c), especially in the original Trajan samples coming from the vaults (samples TRA 14, TRA 19, TRA 24 and TRA 25). Dark brown-to-black scoria fragments are also common in all samples, showing lower porphyritic texture, high porosity (subrounded vesicles are predominant) and colour comparable to the matrix by OM. They are characterized by the diffuse presence of elongated crystals of sanidine. Pores are either filled with acicular zeolite crystals or show reaction rims only.

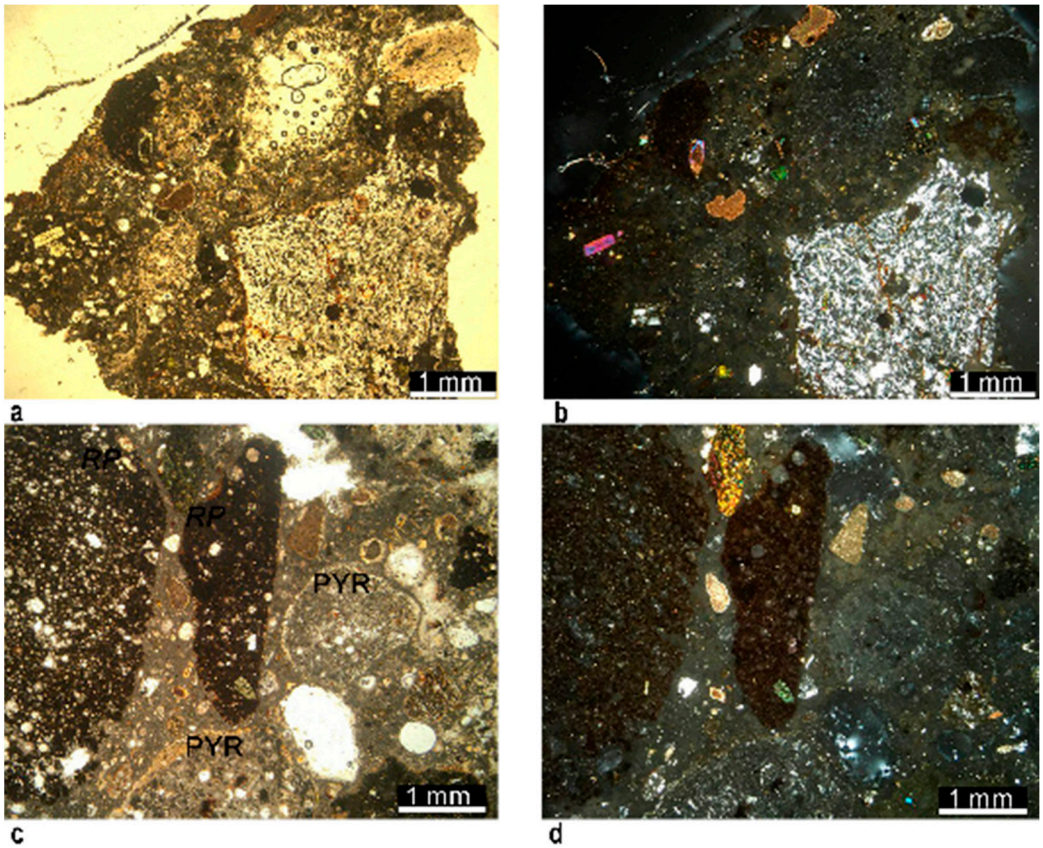

Figure 2. Optical Microscopy micrographs of two Trajan mortars in thin section (parallel (left) and crossed polarized light (right): (**a**,**b**) sample TRA 5; (**c**,**d**) sample TRA 25; PYR = pyroclastic rock fragment surrounded by illuvial clay; RP = red pozzolan.

Additionally, some lava fragments showing analcime replacing leucite, feldspar, sanidine, ilmenite microcrystals and small volcanic rock fragments exhibiting apatite inclusions (Figure 3) were also identified.

Both original and restoration mortars are hydraulic and they are characterized by pozzolanic aggregates that favored the hydraulic reaction [39–41], as constantly found in Roman architecture [31]. In particular, the use of pozzolan is attested starting from 250 BC and the masonry technique of *cocciopesto* has been used since ancient times, probably the 2nd century BC [21,40]. Granular volcanic aggregates are either sand-sized or gravel-sized tephra and they correspond to Vitruvius' *harena fossicia* as described by Jackson et al. [42]. Raw materials at *Aqua Traiana* in fact correspond to highly altered volcanic glass scoriae, hard lavas, dispersed crystals and glassy fragments, frequently highly altered. Even the binder/aggregate ratio (1:3), estimated by petrographic analysis, suggests that Trajan mortars have been produced following Vitruvius' instructions for *harena fossicia*. However, it is now proposed for the first time that *harena fossicia* could possibly be exploited not only from the lithostratigraphic units of the Alban Hills volcano, but also from the deposits of Sabatini Volcanic District.

Trajan samples do not show high porosity (lower than 40%), suggesting that wet concrete could had been pressed to obtain a coherent, well-cemented final product [42]. Additionally, their grey-to-white colour may suggest the washing of pozzolanic aggregates to remove dirt and dust before their addition to the mortar [21]. These features are comparable with the original description by Van Deman [43], later confirmed by Jackson et al. [41], of high-quality mortars produced for monumental buildings during the Trajan era, such as the Trajan Market and the Baths. Moreover, lime lumps do not occur in the Trajan Age mortars of the present study, testifying great knowledge of the manufacturing process and high control of each step [44]. This considerable expertise is even attested by a deep knowledge

of supplies and by precise mixing and selection of the raw materials, strongly depending on the mortar function: lighter aggregates in fact predominate on the vaults. Specifically, the occurrence of red pozzolan (dark-red scoria fragments with starry leucite) was only documented in the Trajan mortars used to build the upper elements of *Aqua Traiana*. This is in agreement with coeval technological choices: at the Trajan's Baths, which indeed followed Domitian's building procedures [42,45,46], but also in the lightened mortars of the vault of "Aula Grande" at the Markets of Trajan [47] and of the "Sala Trisegmentata" at the Forum of Trajan [48].

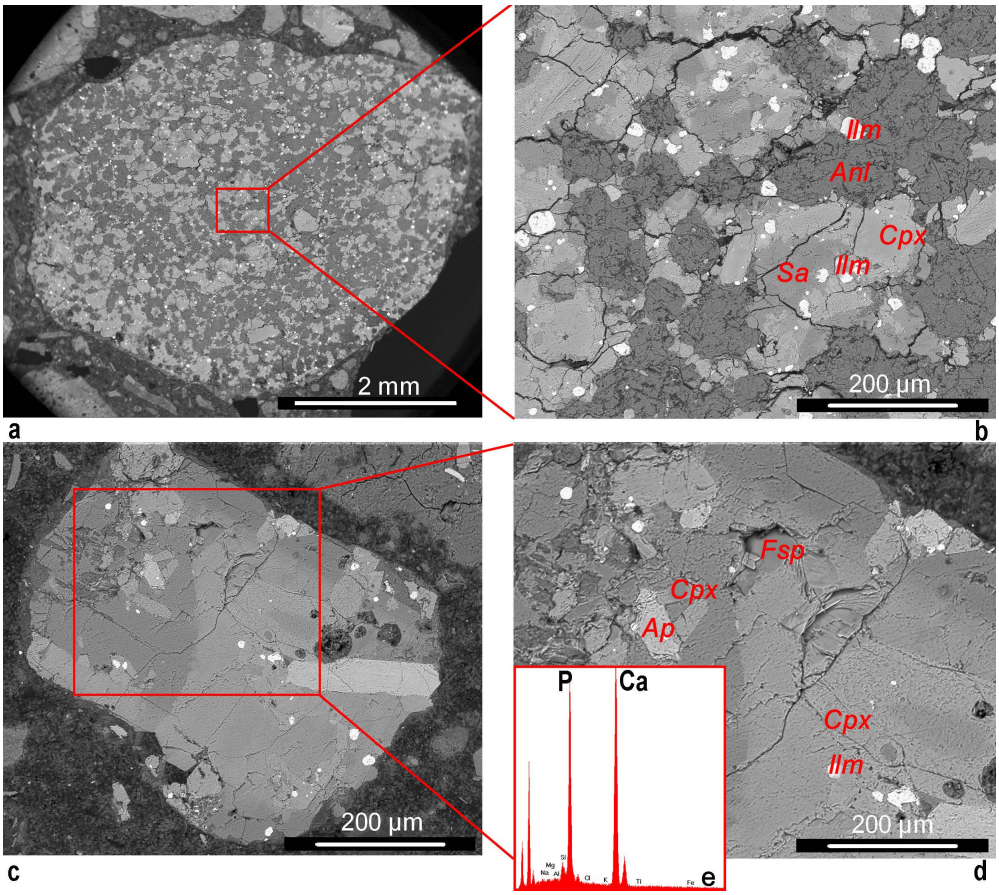

Figure 3. Scanning Electron Microscopy (SEM) micrographs from sample TRA 23: lava fragment (**a**) and a magnified view of the red area (**b**) showing analcime (Anl) replacing leucite, clinopyroxene (Cpx), sanidine (Sa) and ilmenite (Ilm) microcrystals; volcanic rock fragment (**c**) and the red area (**d**) at a higher magnification, with microcrystals of clinopyroxene (Cpx), apatite (Ap), recognized by the contemporary presence of P and Ca in the Energy Dispersive X-ray Spectroscopy spectrum (**e**), feldspar (Fsp) and ilmenite (Ilm).

EMP analysis was performed to identify specific mineral phases that could be useful to characterize the aggregate and reconstruct the possible provenance of raw material. Therefore, aggregates were analyzed to obtain the chemical composition of specific minerals. Particularly, augite crystals analyzed in representative samples highlighted enrichment in Fe. Figure 4 shows an augite crystal in the Trajan sample TRA 11, whose composition (Table 3) is representative of the augite crystals also found and analyzed in the other samples.

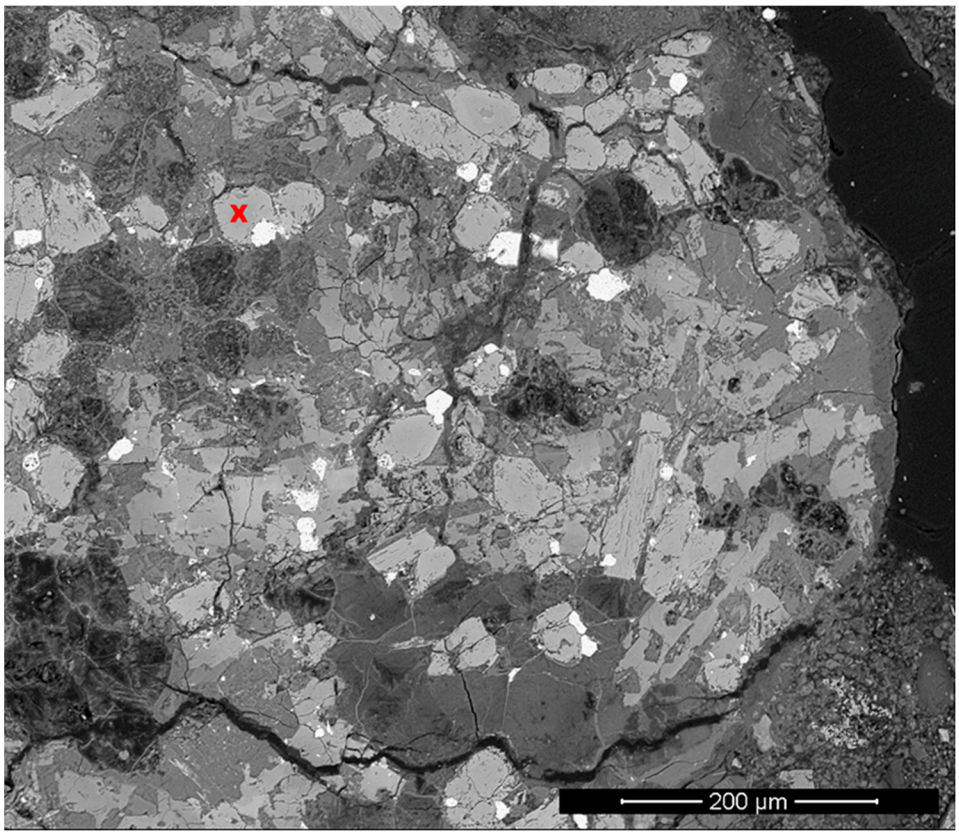

Figure 4. Representative augite crystal in a volcanic rock fragment of the Trajan sample TRA 11 identified by SEM (red cross, see Table 3 for chemical data); in the same micrograph, acicular crystals filling porosities can be also seen.

Table 3. Chemical composition of the representative augite crystal of Figure 4 The relative formula was calculated on 6 oxygens from Electron Microprobe analysis (EMPA).

Oxide	wt% *		apfu
SiO_2	44.66	Si	1.680
Al_2O_3	7.64	Al	0.339
MgO	10.10	Mg	0.567
Cr_2O_3	0.00	Cr^{+3}	0.000
TiO_2	1.37	Ti	0.039
FeO	11.27	Fe^{+2}	0.086
Fe_2O_3	0.00	Fe^{+3}	0.268
MnO	0.27	Mn	0.009
CaO	24.02	Ca	0.968
Na_2O	0.53	Na	0.038
K_2O	0.13	K	0.006
Total	100	Cat. Sum	4.000

* normalized to 100.

Additionally, in these pyroclastic rock fragments, secondary minerals also occurred (analcimised leucite) and porosities were filled with recrystallized zeolite. These crystals were very fine, with a thickness lower than 5 µm, therefore only one measurement could be performed on each crystal. However, numerous (more than three for each sample) point analyses were performed to evaluate the chemical composition of zeolites, according to [49]. By EMPA, these acicular crystals were identified as Mg-enriched chabazite (Table 4).

Table 4. Chemical composition and relative formula, calculated on 24 oxygens and 12 H_2O molecules, of different representative chabazite crystals identified in different pyroclastic rock fragments.

	TRA 23	**TRA21**	**TRA11**		**TRA 23**	**TRA21**	**TRA11**
Oxide		*wt %*		**Element**		*apfu*	
SiO_2	46.807	51.835	55.020	Si	7.962	8.959	8.971
Al_2O_3	21.280	15.019	16.684	Al	4.272	3.063	3.210
				Z-site	**12.234**	**12.022**	**12.182**
CaO	6.553	5.336	4.707	Ca	1.196	0.989	0.823
Na_2O	0.166	0.271	0.205	Na	0.027	0.045	0.032
K_2O	2.023	2.411	2.350	K	0.440	0.532	0.489
MgO	0.888	0.726	0.582	Mg	0.225	0.187	0.142
Total	**77.717**	**75.598**	**79.548**	**X-site**	**1.888**	**1.754**	**1.487**

Pumice clasts in the mortars have a round shape and high porosity, with colour ranging from white to yellow or grey in PPL.

Single crystals such as amphiboles, pyroxenes and feldspars (plagioclase—mainly albite—orthoclase, anorthoclase and sanidine), all attributable to volcanic rock fragments, are dispersed in the binder. Some of them, especially pyroxene and feldspar crystals, sometime show alterations, such as partial dissolution or fractures with recrystallizations.

Fragments of volcanic rocks (leucitite type), with big crystals of leucite, clinopyroxene and plagioclase, were only present in TRA 6 and TRA 34, which were both related to the papal restoration and may imply a slightly different supply.

Grog, namely crushed ceramic fragments, is the only artificial material with pozzolanic behavior identified in the sole sample TRA 34 as predominant, while natural materials with pozzolanic behavior are less common in this sample. The use of ceramic fragments as aggregates in ancient mortar is widely attested [40,50]. The role of ceramics is comparable to that of pozzolan, the vitreous or amorphous fraction reacting with the binder to produce a hard and waterproof material, even if the reaction is not as strong as with pozzolan [38].

The strong compositional difference between papal and Trajan Age samples allows an easy differentiation of the two building phases.

Our results show that the original bedding mortars of the Trajan aqueduct were produced from a mixture of lime, water and fine-grained material with pozzolanic behavior. The aggregate is exclusively constituted by the natural material of volcanic origin, while artificial components are absent. These major components are typical in the volcanism of the Roman Magmatic Province [51] and compatible with the geological setting of the Sabatini Volcanic District with rocks ranging from leucite-tephrites to leucite- and haüyne-phonolites. Analcime characterizes the secondary assemblage of these volcanic products, being leucite subjected to analcimisation [52], as it is commonly found in lithified deposits of this area [53,54]. Microsubhedral ilmenite has been also described as a typical, ubiquitous accessory mineral in the Sabatini dark-grey porphyritic lava fragments [55]. The black fragments in our mortars may indeed correspond to the description given for glassy clasts from the upper lithified deposit of Tufo Rosso a Scorie Nere (red tuff with black scoria) [56]. Finally, the recognition of apatite in some vitreous fragments corroborates the hypothesis of local supply. In fact, apatite occurs as an accessory mineral in the tephriphonolite, latite and phonotephrite of the Martignano Units [57]. The use of this kind of supply is expressed by the compatibility in chemical composition of the clinopyroxenes calculated in the present work and those provided by the literature [55,57,58] in leucite-tephrites from the middle Martignano Unit. However, it must be remarked that apatite has been also found in the low porphyritic scoriae of Pozzolane Nere and Pozzolanelle formations of the Alban Hills [59]. Indeed, the concomitant presence of pozzolanic aggregates from further areas of the Roman Magmatic Province is possible, especially if we consider that in the Roman imperial period the supply from far away quarries had become common [41]. For example, sanidine-bearing pumices, which are frequent aggregates in the mortars from

Aqua Traiana, are also described in the San Paolo formation, deposited by the Tiber River and its tributaries at the base of the Capitoline Hill [41,48].

Independently of the nature of the aggregate and binder, needle-shaped recrystallizations occurred in the pores. These recrystallizations were also found in local tuffs [60,61]. However, chabazite in the present work showed a slightly higher Mg content and less K and Na, suggesting the presence of zeolite (phillipsite and chabazite) as the secondary weathering mineral or related to the hydraulic reaction [62–64].

3.2. Bricks and Cocciopesto

Brick samples are characterized by fine grain-sized inclusions and a clayey matrix. The nature of the inclusions, their packing and mean size were considered to distinguish two petrographic fabrics (Table 5).

Table 5. Microscopic characteristics of brick and *cocciopesto* fragments.

Sample	Porosity	Matrix	Inclusions	
TRA 3	5% Meso–macrovesicles	90% non calcareous brown-green activity	5% Equant–elongated; angular–subrounded; open spaced; not aligned	Predominant: quartz (0.1–0.3 mm), feldspars (0.2–0.3 mm) Common: pyroxene (0.3–1.2 mm) Frequent: iron oxide nodules (0.2–1 mm)
TRA 4	10% Micro–macrovesicles Macrovughs	85% non calcareous brown-green activity	5% Equant–elongated; angular–subrounded; open-spaced; not aligned	Predominant: quartz (0.1–0.2 mm) Common: pyroxene (0.5–1.2 mm) Few: iron oxide nodules (0.2–1 mm), quartz (0.3–1.2 mm) Very rare: siliceous rock fragments (1 mm)
TRA 20	5% Meso–microvesicles	90% non calcareous brown-green activity	5% Equant–elongated; angular–subrounded; open-spaced; not aligned	Predominant: quartz (0.1 mm), feldspars (0.2–0.3 mm) Dominant: pyroxene (0.4–1.3 mm) Few: quartz (0.5–1 mm) Very rare: volcanic rock fragments (5 mm)
TRA 26	5% Meso–microvesicles	55% non calcareous red-brown activity	40% Equant–elongated; angular–subrounded; open-spaced; not aligned	Predominant: quartz (0.1–0.3 mm), Few: quartz (0.6–1.3 mm) Rare: pyroxene (0.3–0.5 mm), iron oxide nodules (0.3–0.8 mm)
TRA 29 *	5% Microvesicles	90% non calcareous brown-green activity	5% Equant–elongated; angular–subangular; single-spaced; not aligned	Predominant: quartz (0.1–0.3 mm), Common: pyroxene (0.7–0.8 mm) Few: quartz (0.7 mm) Very rare: fragments of siliceous rocks (1.0 mm), iron oxide nodules (0.3–0.5 mm)
	5% Microvesicles	90% non calcareous brown-green activity	5% Equant–elongated; angular–subangular; single-spaced; not aligned	Predominant: quartz (0.1–0.3 mm), Common: pyroxene (0.6 mm) Very rare: iron oxide nodules (0.3–0.5 mm)

Table 5. *Cont.*

Sample	Porosity	Matrix	Inclusions	
TRA 33 *	3% Microvesicles	92% non calcareous brown-green activity	5% Equant–elongated; angular–subangular; single-spaced; not aligned	Predominant: quartz (0.1–0.3 mm), Few: quartz (0.7–1.3 mm), pyroxene (0.5–0.7 mm) Very rare: iron oxide nodules (0.3–0.7 mm)
	3% Microvesicles meso–macrovughs	87% non calcareous brown-green activity	10% Equant–elongated; angular–subangular; single-spaced; not aligned	Predominant: quartz (0.1–0.3 mm), Common: pyroxene (0.5–1.2 mm) Few: quartz (0.2–0.8 mm), pyroxene (0.4–0.6 mm)
	5% Microvesicles meso–macrovughs	90% non calcareous brown-green activity	5% Equant–elongated; angular–subangular; single-spaced; not aligned	Predominant: quartz (0.1–0.3 mm), Few: quartz (0.5 mm), pyroxene (0.5–0.6 mm)

* TRA 29 and TRA 33 are *cocciopesto* samples where three different brick fragments were recognized and described.

The first *fabric A-matrix* is characterized by a low percentage of inclusions (5%), equant and elongated, from angular to subrounded, open-spaced and not aligned with respect to the margin of the sample. Predominant fine quartz and plagioclase, common pyroxene crystals and iron oxide nodules were identified. In addition, some very rare fragments of rocks were also present. The porosity was estimated to be between 5 and 10% and was mainly represented by mesovesicles and vughs, not aligned and without any secondary calcite. The non-calcareous matrix ranged in colour from beige to brown-green and it was optically active. The results obtained for the samples belonging to *fabric A-matrix* suggest that the starting raw material consisted of a purified clay containing fine quartz, plagioclase and pyroxene inclusions. The material underwent a selection process to remove the coarser fraction, as suggested by the absence of coarse inclusions. This process had good efficiency, as testified by the low percentage of inclusions and by the very fine grain size.

The second *fabric B-inclusions*, including only bipedal samples, was distinguished by the higher percentage (40%) of very fine grain-sized inclusions. Fine quartz is predominant in the samples, whereas coarser crystals were few in the matrix; rare pyroxene and nodules of iron oxides were also identified. The low porosity was represented by meso- and microvesicles without any secondary recrystallization. The non-calcareous matrix had a red-brownish colour and optical activity.

Concerning the *cocciopesto* fragments, the matrix was similar to the amorphous gel-like cementing matrix identified in mortar samples. It was impossible to distinguish crystals and it had very low colours ranging from green to brown. The aggregate was only represented by grog. Its inclusions show a clayey matrix with a brown-greenish colour, optically active. Predominant fine quartz and rare coarser crystals of pyroxene and quartz were identified among aggregates. The porosity was low and both inclusions and pores did not exhibit a preferred alignment. In addition, porosities were filled by secondary calcite.

Fabric B-inclusions could have been produced with a different clay respect to *fabric A-matrix*, the first being characterized by a higher amount of fine quartz and subjected to a lighter purification step during the production.

The difference in the granulometry and percentage of inclusions is probably connected to the end-use of the materials. The *fabric A-matrix* includes brick samples used in the masonry, which are not subjected to continuous attrite, whereas bipedal bricks in *fabric B-inclusions* are typical, squared, Roman bricks with a 60-cm side, used for flooring.

The strong optical activity of the matrix observed in both fabrics gives preliminary information about the firing temperature, which is suggested to be lower than 850 °C [17], in agreement with the literature [65].

The rest of the minerals identified are compatible with the volcanic geological setting of the area, suggesting a local supply of the clay.

Cocciopesto fragments show a matrix similar to the amorphous binder of mortar samples dated to the Trajan Age. The inclusions, only represented by grog, are comparable to the bricks of *fabric A-matrix*. Therefore, a supply of similar raw materials is suggested, and comparable technology and contemporary production are hereby hypothesized.

4. Conclusions

The current research for the first time permitted a complete characterization of the building materials of the ancient *Aqua Traiana* aqueduct.

Concerning the mortars, they are all hydraulic, with fine aggregates of volcanic origin. Specifically, Trajan Age samples are characterized by a calcite-free amorphous binder, while a lime binder characterizes the samples of the papal restauration.

The compatibility of the pozzolanic aggregate with local supplies from the Bracciano area is for the first time inferred; however, supplies from more distant areas of the Roman Magmatic Province are co-occurrent. Raw materials are likely described as Vitruvius' *harena fossicia* and their use is highly compatible with the building technology of the Trajan Era, with specific aggregates for different parts of the masonry.

The great differences among Trajan and papal samples documented in this study may allow the future dating of other parts of the aqueduct, based on mineralogical and chemical characterization. Indeed, an increased number of mortar samples will allow collecting a systematic overview of the mineralogical assemblage in the mortars from *Aqua Traiana*. In addition, a multivariate statistical analysis using chemical data may be planned, investigating the role of the elements with lower mobile behavior in surface environments, such as K, Sc, Ga, Rb, Cs, REE and other elements such as Hf, Ta and Th, for a deeper differentiation of mortars.

Concerning ceramic components, bricks were produced with local materials and fired at a low temperature, with specific features connected to the end-use. *Cocciopesto* fragments showed a matrix similar to the amorphous binder of Trajan mortar samples and fragments of bricks as inclusions.

The compatibility of materials used in the production of Trajan mortars, bricks and *cocciopesto* suggests similar technological choices and may be explained by a coeval production. However, further investigation is ongoing and it will include samples from the main ducts of the aqueduct.

Author Contributions: M.B.: Data curation, Investigation, Writing—Original Draft. L.M.: Conceptualization, Funding acquisition, Supervision, Writing—Original Draft. L.C.: Data Curation, Investigation. C.D.V.: Formal analysis, Writing—review and editing. S.M.: Writing—review and editing. All authors have read and agreed to the published version of the manuscript.

Funding: Financial support was provided by "Sapienza" University of Rome–Progetto Ateneo 2019 Medeghini.

Institutional Review Board Statement: Not applicable.

Informed Consent Statement: Not applicable.

Data Availability Statement: All data derived from this research are presented in the enclosed figures and tables.

Acknowledgments: The authors want to express their gratitude to Sovrintendenza Capitolina ai Beni Culturali, in particular to Francesco Maria Cifarelli and Marina Marcelli, who allowed the research on the hydraulic mortars of Trajan's aqueduct; to ACEA ATO 2, Antonio Grosso and Armando Zitelli; to Roma Sotterranea speleological association, and in particular to Elettra Santucci, who lead us inside the aqueduct for the sampling. The authors thank the five anonymous reviewers for the useful comments and suggestions on ways to improve the manuscript.

Conflicts of Interest: The authors declare no conflict of interest.

References

1. Botticelli, M.; Mignardi, S.; De Vito, C.; Liao, Y.; Montanari, D.; Shakarna, M.; Nigro, L.; Medeghini, L. Variability in pottery production at Khalet al-Jam'a necropolis, Bethlehem (West Bank): From the Early-Middle Bronze to the Iron Age. *Ceram. Int.* **2020**, *46*, 16405–16415. [CrossRef]
2. Rispoli, C.; Esposito, R.; Guerriero, L.; Cappelletti, P. Ancient Roman mortars from Villa del Capo di Sorrento: A multi-analytical approach to define microstructural and compositional features. *Minerals* **2021**, *11*, 469. [CrossRef]
3. Botticelli, M.; Maras, A.; Candeias, A. μ-Raman as a fundamental tool in the origin of natural or synthetic cinnabar: Preliminary data. *J. Raman Spectrosc.* **2020**, *51*, 1470–1479. [CrossRef]
4. Bandiera, M.; Verità, M.; Lehuédé, P.; Vilarigues, M. The technology of copper-based red glass sectilia from the 2nd century AD Lucius Verus Villa in Rome. *Minerals* **2020**, *10*, 875. [CrossRef]
5. Sanjurjo-Sánchez, J.; Trindade, M.J.; Blanco-Rotea, R.; Garcia, R.B.; Mosquera, D.F.; Burbidge, C.; Prudêncio, M.I.; Dias, M.I. Chemical and mineralogical characterization of historic mortars from the Santa Eulalia de Bóveda temple, NW Spain. *J. Archaeol. Sci.* **2010**, *37*, 2346–2351. [CrossRef]
6. Sánchez-Pardo, J.C.; Blanco-Rotea, R.; Sanjurjo-Sánchez, J.; Barrientos-Rodríguez, V. Reusing stones in medieval churches: A multidisciplinary approach to San Martiño de Armental (NW Spain). *Archaeol. Anthropol. Sci.* **2019**, *11*, 2073–2096. [CrossRef]
7. Ricca, M.; Paladini, G.; Rovella, N.; Ruffolo, S.A.; Randazzo, L.; Crupi, V.; Fazio, B.; Majolino, D.; Venuti, V.; Galli, G.; et al. Archaeometric characterisation of decorated pottery from the archaeological site of Villa dei Quintili (Rome, Italy): Preliminary study. *Geosciences* **2019**, *9*, 172. [CrossRef]
8. Maltoni, S.; Silvestri, A. A mosaic of colors: Investigating production technologies of Roman glass tesserae from Northeastern Italy. *Minerals* **2018**, *8*, 255. [CrossRef]
9. Rahim, N.S.A. Analytical study and conservation of archaeological terra sigillata ware from Roman period, Tripoli, Libya. *Sci. Cult.* **2016**, *2*, 19–27. [CrossRef]
10. Maritan, L. Archaeo-ceramic 2.0: Investigating ancient ceramics using modern technological approaches. *Archaeol. Anthropol. Sci.* **2019**, *11*, 5085–5093. [CrossRef]
11. Jackson, M.; Marra, F. Roman stone masonry: Volcanic foundations of the ancient city. *Am. J. Archaeol.* **2006**, *110*, 403–436. [CrossRef]
12. Benjelloun, Y.; de Sigoyer, J.; Dessales, H.; Garambois, S.; Şahin, M. Construction history of the aqueduct of Nicaea (Iznik, NW Turkey) and its on-fault deformation viewed from archaeological and geophysical investigations. *J. Archaeol. Sci. Rep.* **2018**, *21*, 389–400. [CrossRef]
13. Maravelaki-Kalaitzaki, P.; Galanos, A.; Doganis, I.; Kallithrakas-Kontos, N. Physico-chemical characterization of mortars as a tool in studying specific hydraulic components: Application to the study of ancient Naxos aqueduct. *Appl. Phys. A* **2011**, *104*, 335–348. [CrossRef]
14. Figueiredo, M.O.; Veiga, J.P.; Silva, T.P. Materials and reconstruction techniques at the Aqueduct of Carthage since the Roman period. *Hist. Constr. Guimares* **2001**, *1*, 391–400.
15. Maritan, L.; Mazzoli, C.; Sassi, R.; Speranza, F.; Zanco, A.; Zanovello, P. Trachyte from the Roman aqueducts of Padua and Este (north-east Italy): A provenance study based on petrography, chemistry and magnetic susceptibility. *Eur. J. Miner.* **2013**, *25*, 415–427. [CrossRef]
16. Rizzo, G.; Ercoli, L.; Megna, B.; Parlapiano, M. Characterization of mortars from ancient and traditional water supply systems in Sicily. *J. Therm. Anal. Calorim.* **2008**, *92*, 323–330. [CrossRef]
17. Medeghini, L.; Ferrini, V.; Di Nanni, F.; D'Uva, F.; Mignardi, S.; De Vito, C. Ceramic pipes of the Roman aqueduct from Raiano village (L'Aquila, Italy): A technological study. *Constr. Build. Mater.* **2019**, *218*, 618–627. [CrossRef]
18. Dembskey, E.J. The Aqueducts of Ancient Rome. Ph.D. Thesis, University of South Africa, Pretoria, South Africa, 2009.
19. Cifarelli, F.M.; Marcelli, M. L'Aqua Traiana: Infrastruttura della città antica e moderna. In *Traiano: Costruire L'Impero, Creare L'Europa*; Parisi Presicce, C., Milella, M., Pastor, S., Eds.; De Luca Editori d'Arte: Rome, Italy, 2017; pp. 221–226.
20. O'Neill, E. L'Acquedotto di Traiano tra il ninfeo di S. Fiora e il Lago di Bracciano. *Atlante Temat. Topogr. Antica* **2014**, *24*, 197–214.
21. Lancaster, L.C. *Concrete Vaulted Construction in Imperial Rome: Innovations in Context*; Cambridge University Press: New York, NY, USA, 2005; ISBN 9780511610516.
22. Marra, F.; Sottili, G.; Gaeta, M.; Giaccio, B.; Jicha, B.; Masotta, M.; Palladino, D.M.; Deocampo, D.M. Major explosive activity in the Monti Sabatini Volcanic District (central Italy) over the 800–390 ka interval: Geochronological–geochemical overview and tephrostratigraphic implications. *Quat. Sci. Rev.* **2014**, *94*, 74–101. [CrossRef]
23. Conticelli, S.; Peccerillo, A. Petrology and geochemistry of potassic and ultrapotassic volcanism in central Italy: Petrogenesis and inferences on the evolution of the mantle sources. *Lithos* **1992**, *28*, 221–240. [CrossRef]
24. Peccerillo, A. Multiple mantle metasomatism in central-southern Italy: Geochemical effects, timing and geodynamic implications. *Geology* **1999**, *27*, 315–318. [CrossRef]
25. Conticelli, S.; D'Antonio, M.; Pinarelli, L.; Civetta, L. Source contamination and mantle heterogeneity in the genesis of Italian potassic and ultrapotassic volcanic rocks: Sr-Nd-Pb isotope data from Roman Province and Southern Tuscany. *Mineral. Petrol.* **2002**, *74*, 189–222. [CrossRef]
26. Conticelli, S.; Avanzinelli, R.; Ammannati, E.; Casalini, M. The role of carbon from recycled sediments in the origin of ultrapotassic igneous rocks in the Central Mediterranean. *Lithos* **2015**, *232*, 174–196. [CrossRef]

27. Masotta, M.; Gaeta, M.; Gozzi, F.; Marra, F.; Palladino, D.M.; Sottili, G. H_2O- and temperature-zoning in magma chambers: The example of the Tufo Giallo della Via Tiberina eruptions (Sabatini Volcanic District, central Italy). *Lithos* **2010**, *118*, 119–130. [CrossRef]
28. Buttinelli, M.; De Rita, D.; Cremisini, C.; Cimarelli, C. Deep explosive focal depths during maar forming magmatic-hydrothermal eruption: Baccano Crater, Central Italy. *Bull. Volcanol.* **2011**, *73*, 899–915. [CrossRef]
29. Sottili, G.; Palladino, D.M.; Marra, F.; Jicha, B.; Karner, D.B.; Renne, P. Geochronology of the most recent activity in the Sabatini Volcanic District, Roman Province, central Italy. *J. Volcanol. Geotherm. Res.* **2010**, *196*, 20–30. [CrossRef]
30. Marra, F.; Anzidei, M.; Benini, A.; D'Ambrosio, E.; Gaeta, M.; Ventura, G.; Cavallo, A. Petro-chemical features and source areas of volcanic aggregates used in ancient Roman maritime concretes. *J. Volcanol. Geotherm. Res.* **2016**, *328*, 59–69. [CrossRef]
31. Pecchioni, E.; Fratini, F.; Cantisani, E. *Atlas of the Ancient Mortars in Thin Section under Optical Microscope*; Nardini Editore: Firenze, Italy, 2017.
32. Consiglio Nazionale delle Ricerche; Istituto Centrale del Restauro. *Normal 12-83-Aggregati Artificiali di Clasti e Matrice Legante non Argillosa*; COMAS Grafica: Rome, Italy, 1983.
33. Whitbread, I.K. *Greek Transport Amphorae: A Petrological and Archaeological Study*; British School at Athens: Athens, Greece, 1995; Volume 4, ISBN 0-904887-13-8.
34. Pouchou, J.L.; Pichoir, F. "PAP" $\phi(\rho z)$ procedure for improved quantitative microanalysis. In *Microbeam Analysis*; Armstrong, J.T., Ed.; San Francisco Press Inc.: San Francisco, CA, USA, 1985.
35. De Vito, C.; Medeghini, L.; Garruto, S.; Coletti, F.; De Luca, I.; Mignardi, S. Medieval glazed ceramic from Caesar's Forum (Rome, Italy): Production technology. *Ceram. Int.* **2018**, *44*, 5055–5062. [CrossRef]
36. Lifshin, E.; Gauvin, R. Minimizing Errors in Electron Microprobe Analysis. *Microsc. Microanal.* **2001**, *7*, 168–177. [CrossRef]
37. Poole, D.M. Progress in the correction for the atomic number effects. In *Quantitative Electron Probe Microanalysis*; Heinrich, K.F.J., Ed.; National Bureau of Standards, Spec. Pub. 298: Washington, WA, USA, 1968; pp. 93–131.
38. Moropoulou, A.; Bakolas, A.; Aggelakopoulou, E. Evaluation of pozzolanic activity of natural and artificial pozzolans by thermal analysis. *Thermochim. Acta* **2004**, *420*, 135–140. [CrossRef]
39. Chiari, G.; Santarelli, M.L.; Torraca, G. Caratterizzazione delle malte antiche mediante l'analisi di campioni non frazionati. *Matariali Strutt. Probl. Conserv.* **1992**, *2*, 111–137.
40. Torraca, G. *Lectures on Materials Science for Architectural Conservation*; Getty Conservation Institute: Los Angeles, CA, USA, 2009; ISBN 978-0-9827668-3-5.
41. Jackson, M.; Deocampo, D.; Marra, F.; Scheetz, B. Mid-Pleistocene pozzolanic volcanic ash in ancient Roman concretes. *Geoarchaeology* **2010**, *25*, 36–74. [CrossRef]
42. Jackson, M.; Marra, F.; Deocampo, D.; Vella, A.; Kosso, C.; Hay, R. Geological observations of excavated sand (harenae fossiciae) used as fine aggregate in Roman pozzolanic mortars. *J. Rom. Archaeol.* **2007**, *20*, 25–53. [CrossRef]
43. Van Deman, E.B. Methods of determining the date of Roman concrete monuments. *Am. J. Archaeol.* **1912**, *16*, 230–251. [CrossRef]
44. Moropoulou, A.; Bakolas, A.; Anagnostopoulou, S. Composite materials in ancient structures. *Cem. Concr. Compos.* **2005**, *27*, 295–300. [CrossRef]
45. Freda, C.; Gaeta, M.; Giaccio, B.; Marra, F.; Palladino, D.M.; Scarlato, P.; Sottili, G. CO_2-driven large mafic explosive eruptions: The Pozzolane Rosse case study from the Colli Albani Volcanic District (Italy). *Bull. Volcanol.* **2011**, *73*, 241–256. [CrossRef]
46. Marra, F.; Danti, A.; Gaeta, M. The volcanic aggregate of ancient Roman mortars from the Capitoline Hill: Petrographic criteria for identification of Rome's "pozzolans" and historical implications. *J. Volcanol. Geotherm. Res.* **2015**, *308*, 113–126. [CrossRef]
47. Jackson, M.D.; Logan, J.M.; Scheetz, B.E.; Deocampo, D.M.; Cawood, C.G.; Marra, F.; Vitti, M.; Ungaro, L. Assessment of material characteristics of ancient concretes, Grande Aula, Markets of Trajan, Rome. *J. Archaeol. Sci.* **2009**, *36*, 2481–2492. [CrossRef]
48. Bianchi, E.; Brune, P.; Jackson, M.; Marra, F.; Meneghini, R. Archaeological, structural, and compositional observations of the concrete architecture of the Basilica Ulpia and Trajan's Forum. *Comm. Hum. Litt.* **2011**, *128*, 73–95.
49. Campbell, L.S.; Charnock, J.; Dyer, A.; Hillier, S.; Chenery, S.; Stoppa, F.; Henderson, C.M.B.; Walcott, R.; Rumsey, M. Determination of zeolite-group mineral compositions by electron probe microanalysis. *Mineral. Mag.* **2016**, *80*, 781–807. [CrossRef]
50. Izzo, F.; Arizzi, A.; Cappelletti, P.; Cultrone, G.; De Bonis, A.; Germinario, C.; Graziano, S.F.; Grifa, C.; Guarino, V.; Mercurio, M.; et al. The art of building in the Roman period (89 B.C.–79 A.D.): Mortars, plasters and mosaic floors from ancient Stabiae (Naples, Italy). *Constr. Build. Mater.* **2016**, *117*, 129–143. [CrossRef]
51. Jackson, M.D.; Marra, F.; Hay, R.L.; Cawood, C.; Winkler, E.M. The judicious selection and preservation of tuff and travertine building stone in ancient Rome. *Archaeometry* **2005**, *47*, 485–510. [CrossRef]
52. Giampaolo, C.; Godano, R.F.; Di Sabatino, B.; Barrese, E. The alteration of leucite-bearing rocks: A possible mechanism. *Eur. J. Mineral.* **1997**, *9*, 1277–1292. [CrossRef]
53. Cappelletti, P.; Petrosino, P.; de Gennaro, M.; Colella, A.; Graziano, S.F.; D'Amore, M.; Mercurio, M.; Cerri, G.; de Gennaro, R.; Rapisardo, G.; et al. The "Tufo Giallo della Via Tiberina" (Sabatini Volcanic District, Central Italy): A complex system of lithification in a pyroclastic current deposit. *Mineral. Petrol.* **2015**, *109*, 85–101. [CrossRef]
54. Hay, R.L.; Sheppard, R.A. Occurrence of zeolites in sedimentary rocks: An overview. *Rev. Mineral. Geochem.* **2001**, *45*, 217–234. [CrossRef]
55. Cundari, A. Petrogenesis of leucite-bearing lavas in the Roman volcanic Region, Italy-The Sabatini lavas. *Contrib. Mineral. Petrol.* **1979**, *70*, 9–21. [CrossRef]

56. Bear, A.N.; Giordano, G.; Giampaolo, C.; Cas, R.A.F. Volcanological constraints on the post-emplacement zeolitisation of ignimbrites and geoarchaeological implications for Etruscan tomb construction (6th–3rd century B.C.) in the Tufo Rosso a Scorie Nere, Vico Caldera, Central Italy. *J. Volcanol. Geotherm. Res.* **2009**, *183*, 183–200. [CrossRef]
57. Del Bello, E.; Mollo, S.; Scarlato, P.; von Quadt, A.; Forni, F.; Bachmann, O. New petrological constraints on the last eruptive phase of the Sabatini Volcanic District (central Italy): Clues from mineralogy, geochemistry, and Sr–Nd isotopes. *Lithos* **2014**, *205*, 28–38. [CrossRef]
58. Sottili, G.; Palladino, D.M.; Gaeta, M.; Masotta, M. Origins and energetics of maar volcanoes: Examples from the ultrapotassic Sabatini Volcanic District (Roman Province, Central Italy). *Bull. Volcanol.* **2012**, *74*, 163–186. [CrossRef]
59. Marra, F.; Karner, D.B.; Freda, C.; Gaeta, M.; Renne, P. Large mafic eruptions at Alban Hills Volcanic District (Central Italy): Chronostratigraphy, petrography and eruptive behavior. *J. Volcanol. Geotherm. Res.* **2009**, *179*, 217–232. [CrossRef]
60. Cappelletti, P.; Langella, A.; Colella, A.; De' Gennaro, R.D.E. Mineralogical and technical features of zeolite deposits from northern Latium volcanic district. *Period. Mineral.* **1999**, *68*, 127–144.
61. Lombardi, G.; Meucci, C. Il Tufo Giallo della Via Tiberina (Roma) utilizzato nei monumenti romani. *Rend. Lincei* **2006**, *17*, 263–287. [CrossRef]
62. Jackson, M.D.; Mulcahy, S.R.; Chen, H.; Li, Y.; Li, Q.; Cappelletti, P.; Wenk, H.R. Phillipsite and Al-tobermorite mineral cements produced through low-temperature water-rock reactions in Roman marine concrete. *Am. Mineral.* **2017**, *102*, 1435–1450. [CrossRef]
63. Jackson, M.D.; Chae, S.R.; Mulcahy, S.R.; Meral, C.; Taylor, R.; Li, P.; Emwas, A.-H.; Moon, J.; Yoon, S.; Vola, G.; et al. Unlocking the secrets of Al-tobermorite in Roman seawater concrete. *Am. Mineral.* **2013**, *98*, 1669–1687. [CrossRef]
64. Jackson, M.D.; Moon, J.; Gotti, E.; Taylor, R.; Chae, S.R.; Kunz, M.; Emwas, A.-H.; Meral, C.; Guttmann, P.; Levitz, P.; et al. Material and elastic properties of Al-tobermorite in ancient Roman seawater concrete. *J. Am. Ceram. Soc.* **2013**, *96*, 2598–2606. [CrossRef]
65. Cairoli, F.G. *L'Edilizia Nell'Antichità*; Carocci Editore: Rome, Italy, 2018.